Data Mining Inspired Localized Resistivity in Global MHD Simulations of the Magnetosphere

H. Arnold[1], K. Sorathia[1], G. Stephens[1], M. Sitnov[1], V.G. Merkin[1], J. Birn[2]

[1]Johns Hopkins Applied Physics Laboratory, Laurel, MD USA
[2]Space Science Institute, Boulder, CO USA

Key Points:

- Localized Resistivity in global MHD simulations can "encourage" magnetic reconnection in specific locations to match data mining results
- Magnetic reconnection at $X_{GSM} \lesssim -20R_E$ can suppress the formation of extended x-lines at $X_{GSM} \gtrsim -15R_E$
- Reconnection outflows rebound from the near-Earth region causing transient and narrow (in Y_{GSM}) secondary reconnection

Corresponding author: Harry Arnold, harryarnold@jhuapl.edu

Abstract

Recent advances in reconstructing Earth's magnetic field and associated currents by utilizing data mining of in situ magnetometer observations in the magnetosphere have proven remarkably accurate at reproducing observed ion diffusion regions. We investigate the effect of placing regions of localized resistivity in global simulations of the magnetosphere at specific locations inspired by the data mining results for the substorm occurring on July 6, 2017. When explicit resistivity is included, the simulation forms an x-line at the same time and location as the MMS observation of an ion diffusion region at 15:35 UT on that day. Without this explicit resistivity, reconnection forms later in the substorm and far too close to Earth ($\gtrsim -15R_E$), a common problem with global simulations of Earth's magnetosphere. A consequence of reconnection taking place farther down the tail due to localized resistivity is that the reconnection outflows transport magnetic flux Earthward and thus prevent the current sheet from thinning enough for reconnection to take place nearer Earth. As these flows rebound tailward from the inner magnetosphere, they can temporarily and locally (in the dawn-dusk direction) stretch the magnetic field allowing for small scale x-lines to form in the near Earth region. Due to the narrow cross-tail extent of these x-lines ($\lesssim 5R_E$) and their short lifespan ($\lesssim$ 5min), they would be difficult to observe with in situ measurements. Future work will explore time-dependent resistivity using 5 minute cadence data mining reconstructions.

Plain Language Summary

[enter your Plain Language Summary here or delete this section]

1 Introduction

Earth's magnetosphere is a dynamic system driven by the solar wind. Magnetic reconnection on the day side transfers magnetic flux to the night side, gradually increasing the magnetic energy density in the tail lobes during the growth phase of a substorm. At some point the expansion phase is explosively triggered, likely due to demagnetization of ions (Schindler, 1974; Sitnov & Schindler, 2010; Sitnov et al., 2013; Bessho & Bhattacharjee, 2014; Pritchett, 2015) or electrons (Coppi et al., 1966; Hesse & Schindler, 2001; Liu et al., 2014), and the stored energy in the lobes is released through magnetic reconnection (Baker & P, 1996; Angelopoulos et al., 2008). This results in the dipolarization of the nightside magnetic field (Russell & McPherron, 1973).

Modelers have successfully simulated many of the observed features of substorms, including magnetotail reconnection and resulting dipolarization (e.g. Birn et al., 1996; Raeder, 2003; Merkin et al., 2019). However, no single simulation can correctly simulate all the physics due to the several orders of magnitude difference between kinetic and global scales. This has led to different efforts to understand the relevant physics, but there are still many questions unanswered. Notably, where and when does magnetic reconnection take place in the magnetotail and how does that affect the global system?

We investigate this question in the context of a global magnetohydrodynamic (MHD) simulation, but also consider the important role non-MHD effects play in determining the location and timing of reconnection in the magnetotail. Prior to reconnection onset, the tail current sheet may have a multiscale structure with an ion-scale thin current sheet embedded in a thicker plasma sheet (Sergeev et al., 2011) or it may be bifurcated on similar ion scales (Nakamura et al., 2002; Runov et al., 2003, 2005, 2006; Sergeev et al., 2003). While Birn and Schindler (2002) have demonstrated that thin current sheets can form even within a quasi-static isentropic model with isotropic pressure (equivalent to slow ideal MHD evolution), other approaches have indicated the possibly important role of pressure anisotropy (Artemyev et al., 2021). Further, during, or even prior to, reconnection the current sheet thins even more down to electron scales (Torbert et al., 2018).

Additionally, several studies indicate that x-lines are commonly expected and observed to be near $-40R_E < X_{GSM} < -20R_E$ (L. Q. Zhang et al., 2010; Nagai et al., 1998; Imber et al., 2022; Zhao et al., 2016). However, extended x-lines are often seen too close to the Earth in global MHD simulations (El-Alaoui et al., 2009; Gong et al., 2021; Bard & Dorelli, 2021; Park, 2021) (see also Fig. 3 (a)) and even in Hall MHD or hybrid simulations (Bard & Dorelli, 2021; Runov et al., 2021).

Recently, data mining (DM) has been harnessed to reconstruct the state of the magnetosphere for a given point in time (G. Stephens et al., 2019). In order to test the accuracy of this method the authors examined $B_{z,GSM} = 0$ contours in the magnetotail current sheet and compared them to Magnetospheric Multiscale Mission (MMS) observations of ion diffusion regions (IDRs). Ions decouple from the magnetic field in IDRs and thus IDRs are useful for identifying features in the magnetic field geometry such as x- and o-lines. The authors were able to show these contours were within $1R_E$ of an MMS identified IDR for 16 out of 26 total IDRs. 8 others were within $1R_E$ of a $2nT$ contour, signifying that DM was close to resolving the reconnection site (G. K. Stephens et al., 2022). This is especially impressive since one of the misses occurred during a time of weak magnetospheric activity and the other was during a gap in solar wind data. By identifying the location of x-lines in the reconstruction and placing localized resistivity in these regions in the MHD simulation, we can effectively take non-MHD physics into account and "encourage" the simulation to form an x-line where and when we expect there to be reconnection from the DM results. Without this intervention the crucial process of tail reconnection will not occur at the correct time or location, which will affect the global response of the magnetosphere.

This paper presents results from different simulations that all model the substorm that took place on July 6, 2017 from approximately 15:35 to 17:00. We demonstrate that a localized resistivity can successfully induce reconnection in different locations in the tail. An unexpected result is that reconnection farther down the tail may actually suppress near-Earth reconnection by transporting magnetic flux there and preventing the current sheet from collapsing. However, due to the 3D nature of the tail, the magnetic field can be stretched again by rebounding flows resulting in smaller, transient x-lines in the near-Earth region. These rebounding flows are a well known feature observationaly (e.g. Ohtani et al., 2009) and have been found in global simulations as well (e.g. Merkin et al., 2019). However, the additional reconnection they can create has not yet been discussed.

In section 2 we describe the simulations that we examine and the methodology for identifying x-lines in our simulations. In section 3 we show that DM inspired localized resistivity can create x-lines that match observations. In section 4 we explain how reconnection farther in the tail suppresses extended x-line near Earth. In section 5 we present evidence of small x-lines that from in rebounding flows. And in section 6 we conclude.

2 Event Description and Simulation Setup

We perform simulations using the global magnetohydrodynamic code GAMERA (B. Zhang et al., 2019; Sorathia et al., 2020) coupled with the ionospheric potential solver REMIX (Merkin & Lyon, 2010), which used a constant conductance of $5S$. Our simulations consist of a distorted spherical grid and a cylinder as the boundary with the faces located at $X_{SM} = 30R_E$ and $X_{SM} = -330R_E$. The radius of the cylinder is $110R_E$ and it consists of 96x96x128 grid cells in the radial, polar, and azimuthal dimensions respectively.This leads to a grid cell of length $\sim 0.5R_E$ at $X_{GSM} = -20R_E$. The magnetosphere is driven using data from the OMNI database for the period on July 6, 2017 from 14:35-17:35. The Sym-H magnitude remained small for the entirety of the simulation indicating that the ring current is not important to magnetospheric dynamics. Prior to the simulation, there is a spin-up period of two hours where a dipole magnetosphere

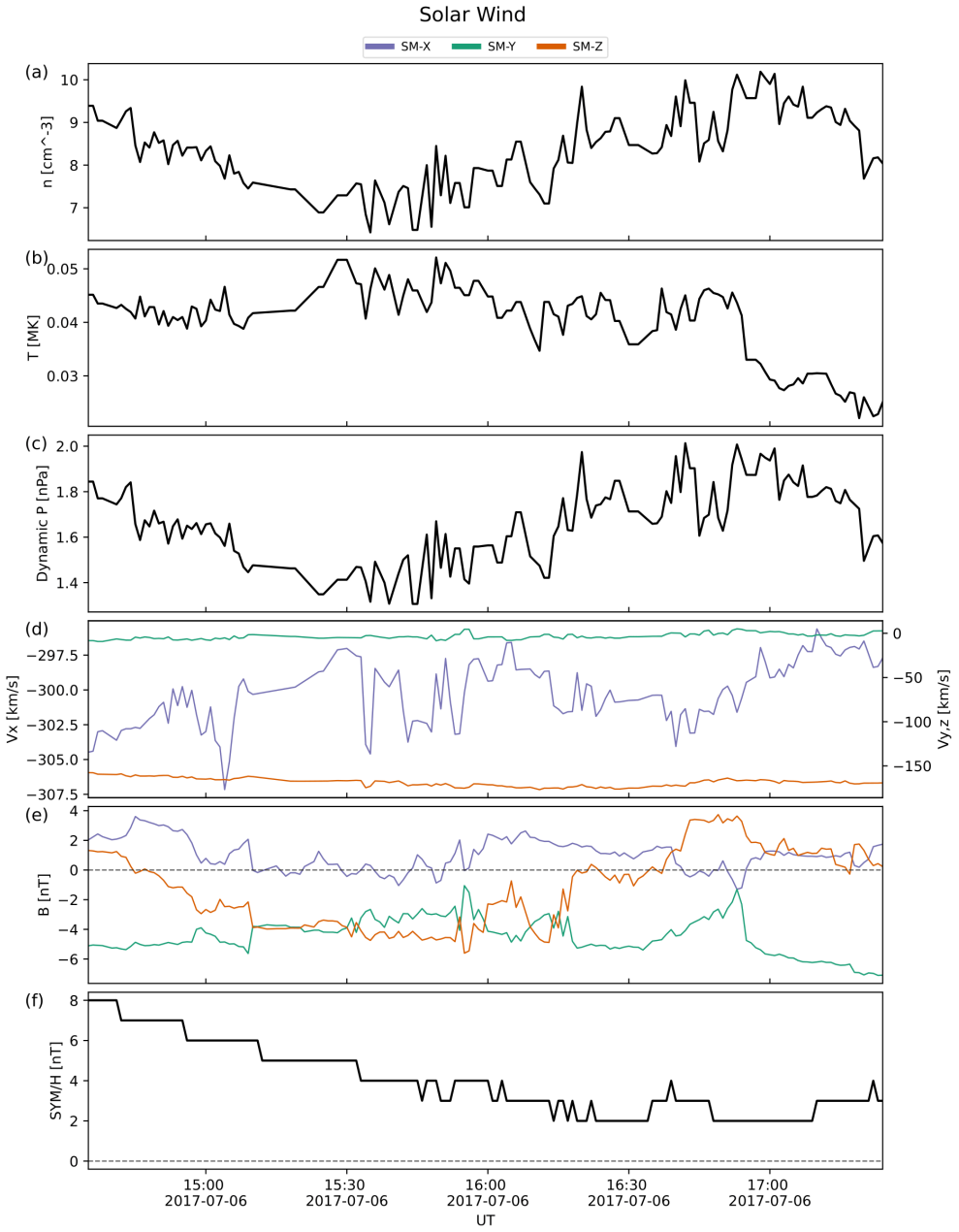

Figure 1. Solar wind parameters from the National Aeronautics and Space Administration OMNI database for the period of our simulations. (a) density, (b) temperature, (c) dynamic pressure, (d) flow velocity, (e) magnetic field, and (f) SYM-H index. The vector quantities are in Solar Magnetic Coordinates.

is driven by a hydrodynamic solar wind corresponding to the initial values on the left side of Fig. 1. All of our simulations result in substorm dynamics due to the southward turning IMF magnetic field.

In this paper we examine 3 simulations: one with no explicit resistivity (Run Base), one with localized resistivity placed near $X_{GSM} \sim -30R_E$ (Run Mid) and one with localized resistivity placed at a location inspired from DM results (Run DM). The location is specified by X_{SM}, Y_{SM}, and Z_{SM} coordinates with varying widths in each direction. The resistivity in our simulations is defined as

$$\eta = \eta_0 / \cosh^2\left(\frac{x - x_0}{L_x} + \frac{y - y_0}{L_y} + \frac{z - z_0}{L_z}\right) \tag{1}$$

where x_0, y_0, and z_0 give the center of the resistive region in SM coordinates, $\eta_0 = 40,000\Omega m$ as in (Hesse & Birn, 1994), $L_x, L_y, L_z = 5, 20, 25R_E$ for Run Mid, and $L_x, L_y, L_z = 6, 10, 4R_E$ for Run DM. Calculating the relevant scales from Run Mid in the resistive region, we find a length of $\sim 1R_E$ for the width of the current sheet in the Z_{GSM} direction, and a characteristic upstream Alfvén speed of $\sim 1000km/s$ which gives a Lundquist number of $S = LU\mu_0/\eta \sim 200$ where μ_0 is vacuum permeability. We also decreased this value of resistivity in a separate simulation (not shown) by an order of magnitude, and in that case the localized region of resistivity was unable to lead to substantial reconnection.

In order to explore the effects of resistivity, we developed a method to identify the location of x-lines. Since we are primarily interested in tail reconnection, we limited ourselves to the region $-60 < X_{GSM}/R_E < -5$, $-10 < Y_{GSM}/R_E < 10$, and $-10 < Z_{GSM}/R_E < 10$. Further, we required that the azimuthal current (in GSM coordinates) be larger than $\sim 0.5A/m^2$ and that both $B_{Z,GSM}$ and $B_{X,GSM}$ reverse sign within 1 grid cell of the suspected x-line location. Then we trace the magnetic field lines for $3R_E$ in the $X_{GSM}-Z_{GSM}$ plane, both parallel and anti-parallel to $\boldsymbol{B}$, starting at $X_{GSM} \pm 1R_E$ from the identified cell. The result is 4 different locations where both ends of the field line that started on the Earthward side of the cell in question will remain on the Earthward side and similarly for the tailward side if the identified cell is an x-line. However, we only require 3 of the final locations to follow this pattern as the reconnecting magnetic field is not guaranteed to perfectly lie along X_{GSM}. The resulting identified x-lines have been verified to have a general agreement with the expected geometry. However, they tend to be spread out in the X_{GSM} and Y_{GSM} directions in the vicinity of an x-line which introduces some unavoidable error.

3 Localized Resistivity Induces Reconnection

There have been many studies of the magnetotail with resistive MHD simulations, and in particular MHD simulations with localized patches of resistivity (Hesse & Birn, 1994; Raeder et al., 1996; Raeder, 1999; Raeder et al., 2001; Birn & Hesse, 2013). These have shown that a localized region of resistivity can induce reconnection locally (Ugai & Tsuda, 1979; Min et al., 1985; Scholer & Otto, 1991). However, until now there has been no way to inform the simulation about where and when reconnection should take place in the magnetotail. Using the magnetosphere reconstruction results from DM, we can determine the location of reconnection with reasonable accuracy. And by strategically placing localized resistivity we will be able to induce reconnection that approximately matches both the spatial and temporal profiles of real x-lines in a given substorm according to DM reconstructions.

As a first step we looked at the x-line that was identified by the MMS on July 6, 2017 at $[X_{GSM}, Y_{GSM}, Z_{GSM}] = [-24.1, 1.41, 4.44]R_E$ (Rogers et al., 2019). In order to match the location of the observed x-line, we placed a region of resistivity as described above to induce reconnection in the appropriate place as determined from DM. The comparison with the simulation without resistivity as well as the DM results can be seen in

Fig. 2. Panel (a) shows the DM results in the $X'_{GSM}-Z_{GSM}$ plane, (b) is the DM results in the $X_{GSM}-Y_{GSM}$ plane, (c) is at the same time but from Run Base in the $X_{GSM}-Z_{GSM}$ plane, (d) is in the $X_{GSM}-Y_{GSM}$ plane, and (e)-(f) are the same as (c)-(d) but from Run DM. The result is a significant difference in the development of the magnetosphere. While both simulations form an x-line deep in the tail near $X_{GSM} \sim -40R_E$ on the dawn side, only the simulation with a localized resistivity leads to reconnection geometry with outflows near $\sim -25R_E$ in excellent agreement with in situ observations.

4 Mid-Tail Reconnection Suppresses Near Earth Reconnection

The above demonstrates that we can induce reconnection with localized resistivity. In the previous section we showed that we can match observations of ion diffusion regions with x-lines in a simulation at the correct place and time. However, to consider a more generalized case, we also look at a simulation with resistivity located in the region $X_{GSM} \sim -30R_E$, Run Mid. This is because of observations suggesting this as the likely location of near Earth reconnection (Imber et al., 2022; Zhao et al., 2016) as well as the consistent and extended x-lines that the DM results suggest exist here (G. K. Stephens et al., 2022), thus Run Mid is also inspired by DM results. A snapshot of Run Base compared with Run Mid and Run DM can be seen in Fig. 3. An important consequence is that the resistivity induced reconnection in both Run Dm and Run Mid creates diverging flows sooner. The Earthward flow transports flux to the near Earth region which prevents the current sheet form narrowing and thus suppresses near Earth reconnection that would otherwise take place. This is especially evident in Run Mid, but even in Run DM the x-lines are generally deeper in the tail. This process is what dipolarizes the inner magnetosphere and naturally prevents reconnection there.

Without explicit resistivity any reconnection in this region (near $X_{GSM} \lesssim -30R_E$) is unsteady and is not extended along the dawn-dusk region. Fig. 4 illustrates this point quite clearly. To form this figure we group all identified x-lines within $2R_E$ of each other, take the average X_{GSM} location, calculate the extent in the dawn dusk direction as the width, and the center in the dawn dusk direction as the Y_{GSM} location. Thus each "x" is colored according to its Y_{GSM} location, plotted according to the time it occurred and its X_{GSM} location, and the size illustrates its width. We show the results for all three simulations. Finally, the observed AL index is also plotted for reference. Interestingly, all simulations form x-lines in the midtail region (near $X_{GSM} \sim -30R_E$) before the substorm onset. However, in Run Base and Run DM the x-lines are smaller in width, tend to drift tailward, and seemingly jump around in X_{GSM}. Shortly after the growth phase begins, an extended x-line forms in the near Earth region for Run Base, initially on the dusk side, and gradually retreats in the expansion phase.

For Run DM the resistivity induces reconnection on the dusk side near $X_{GSM} \sim -20R_E$ just before the start of the growth phase. As the substorm progresses, the x-line gradually extends farther and farther towards the dawn until it occupies most of the tail as can be seen in Fig. 3 (d). This stretching of the x-line is also why the x-line appears to approach Earth. In fact, the x-line on the dusk side stays within the region of resistivity at $X_{GSM} \sim -20R_E$, but approaches Earth on the dawn side. Note that even though the average X_{GSM} position approaches Earth, it still generally stays farther in the tail than in Run Base, especially near the midnight line and duskward as can be seen in Fig. 3. The x-line then retreats and eventually breaks up in the the recovery phase.

By placing resistivity farther in the tail we initially see a similar result. The x-line forms, but then extends in the dawn dusk direction, and stays roughly constant well into the expansion phase. While this x-line stays roughly centered on the midnight line, it extends well into both the dawn and dusk sides. It is likely that the x-line is matching the region of resistivity as expected. Near the recovery phase the x-line finally begins to breakup before effectively disappearing altogether.

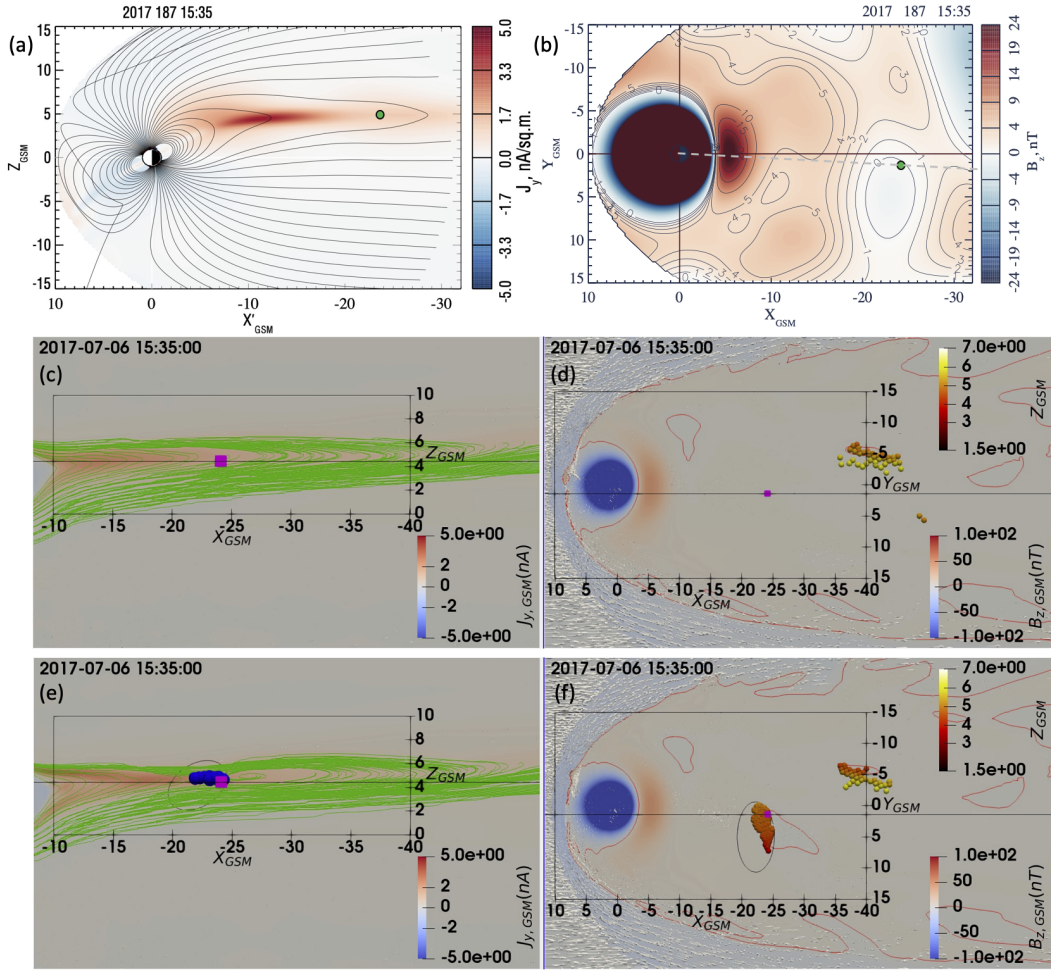

Figure 2. Each figure corresponds to July 6, 2017 at 15:35. Panel (a) and (b) show the DM reconstruction of the magnetosphere in the $X'_{GSM} - Z_{GSM}$ and $X_{GSM} - Y_{GSM}$ ($Z_{GSM} = 4.2R_E$) planes respectively. (a) is the current in the Y_{GSM} direction with field lines in black. (b) is $B_{Z,GSM}$ with contours equal to $B_{Z,GSM} = 0, 2, 3$ and $4nT$. The location of MMS is depicted by a green circle in both panels where it observed an ion diffusion region. The dashed line in (b) shows the location of the plane of (a) and the X'_{GSM} axis. Panels (c) and (d) are the $X_{GSM} - Z_{GSM}$ and $X_{GSM} - Y_{GSM}$ plane respectively from Run Base. (c) shows $J_{Y,GSM}$ with selected field lines in green, and (d) shows $B_{Z,GSM}$ with contours of $B_{Z,GSM} = 0$ in red. Both panels show flow vectors as white arrows. The horizontal lines in each plane corresponds to the location of the plane in the other panel. The pink squares are the location of MMS. The circles are the location of identified x-lines in the simulation, in (d) and (f) they are colored according to their Z_{GSM} location. (c) and (e) only show identified x-lines within $1R_E$ of the plane. Panels (e) and (f) are the same as (c) and (d) respectively except for Run DM. The black circles correspond to contours of resistivity equal to $10,000\Omega m$.

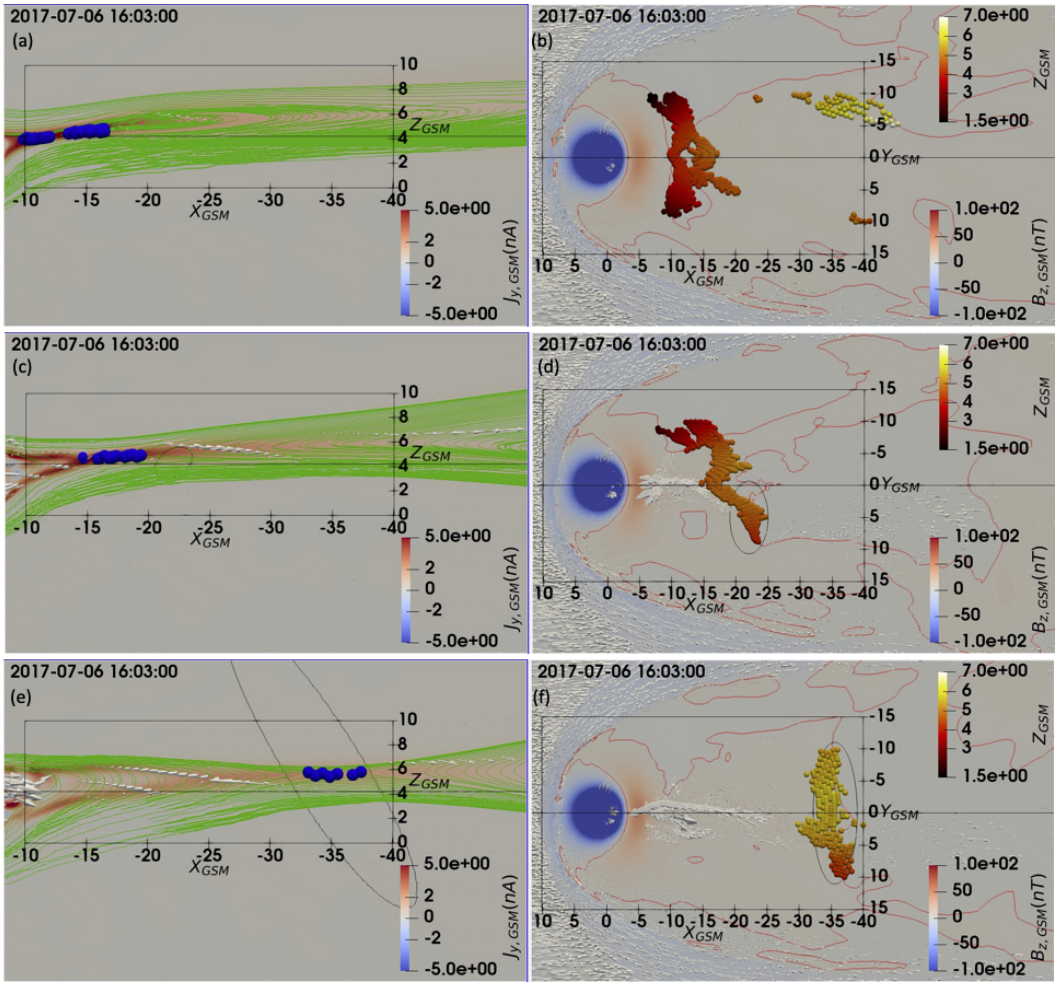

Figure 3. Each pair of panels in this figure have the same format as Fig. 2 (c)-(d). However, they are at a time shortly after reconnection begins in Run Base and they lack the location of MMS. (a) and (b) are from Run Base, (c) and (d) are from Run DM and (e) and (f) are from Run Mid.

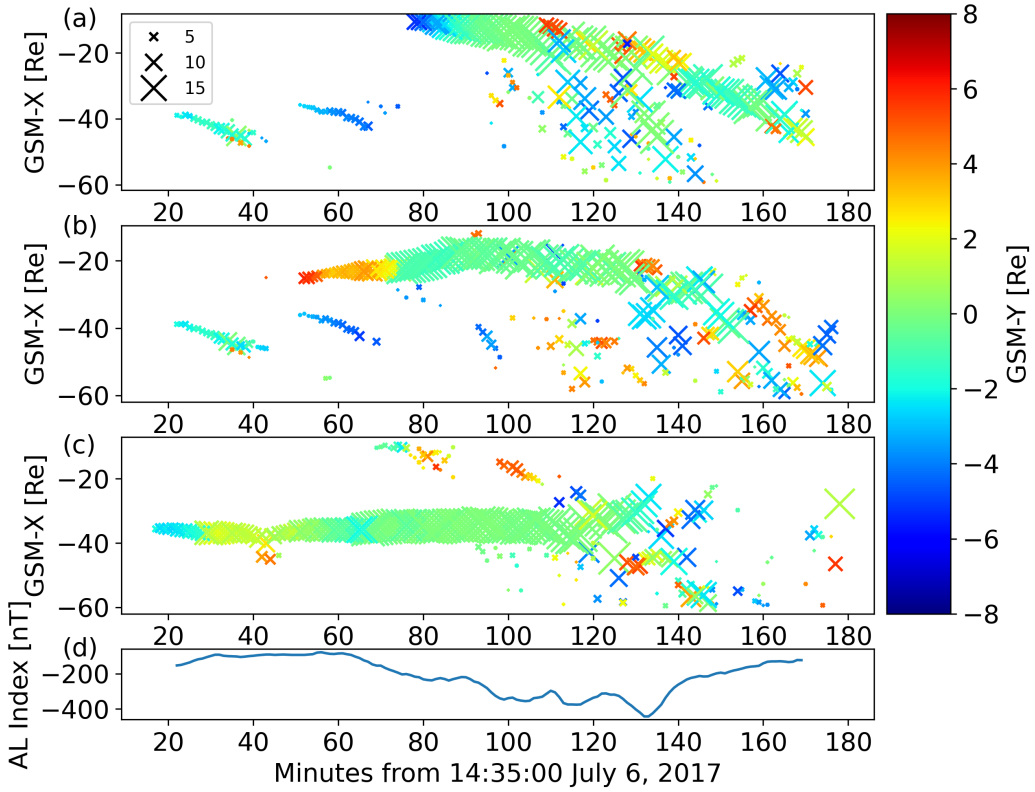

Figure 4. Panel (a) shows the x-lines seen throughout Run Base. Each "x" represents all identified x-lines within $2R_E$ of each other. The legend relates the size of each "x" to the width in the dawn-dusk direction in R_E. The color indicates the center of the x-line in the dawn-dusk direction. Panels (b) and (c) are the same as (a) but for Run DM and Run Mid respectively. Panel (d) is the observed AL index during this time period.

5 Rebounding Flows Stretch the Tail and Create Secondary X-Lines

The previous section clearly described how reconnection farther in the tail suppresses reconnection closer to Earth. However, as can be seen in Fig. 4 (c) there are some near Earth x-lines. These x-lines differ qualitatively from the near Earth x-lines in Run Base. Crucially, these x-lines do not last as long nor do they spread as far in the dawn-dusk direction. Additionally, they tend to form in rebounding flows. Rebounding flows are Earthward flows from reconnection that rebound tailward due to the strong magnetic field near Earth (Ohtani et al., 2009).

As an example of one of these x-lines in Run Mid consider Fig. 5. Panels (a) and (b) are similar to Fig. 3 (c) and (d) but zoomed in and at a different time. This is taken right after the x-line forms and clearly demonstrates that it forms in the tailward flow region as the reconnection outflow rebounds near Earth. Panels (c)-(f) depict various quantities as measured at one of the actual positions that the x-line forms, $[x, y, z] = [-11.05, .5, 4.31]$. However, since the x-line is tilted with respect to the x-axis as can be seen in panel (a), we define $B_{x,r}$ and $B_{z,r}$ to be the reconnecting and reconnected component of the magnetic field respectively. The vertical red dashed line indicates when the flow switches from Earthward to tailward and the vertical green line indicates when reconnection is observed. Shortly after the flow turns tailward the field lines continue to stretch as can be seen in the reduction of $B_{z,r}$ leading to secondary reconnection. These secondary x-lines were also observed in Run DM as can be seen by the small red "x"s in Fig. 4 (b). This suggests that this secondary reconnection may be a common consequence of midtail reconnection.

6 Conclusion

In this paper we have demonstrated the ability to induce reconnection in a global simulation of Earth's magnetosphere. We did not address the physics of why and how reconnection was initiated at a particular location but rather imposed localized resistivity as a means to initiate it in agreement with in situ observations of MMS. This is an important first step towards incorporating real observations into simulations to study a more accurate depiction of substorms. With the DM results we can determine places where x-lines actually form during a substorm and place time dependent patches of local resistivity to induce reconnection at correct locations in a global simulation. This is important since global simulations, and in particular MHD simulations, are missing key kinetic physics which play an important role in determining the specifics of reconnection. However, the recent results demonstrating the accuracy of DM based reconstructions of the magnetosphere allow us to implicitly incorporate otherwise missing physics and correctly simulate the location of reconnection for a given substorm. Future work will include incorporating the time dependent motion of x-lines into our global simulation model.

Without any explicit resistivity, an extended x-line often forms far too close to Earth than we would expect (El-Alaoui et al., 2009; Gong et al., 2021; Bard & Dorelli, 2021; Park, 2021; Runov et al., 2021). This is a common problem in global simulations of the magnetosphere. Interestingly, by placing resistivity farther in the tail and inducing reconnection there, we implicitly suppress reconnection near Earth. This can be explained simply by noting that reconnection farther in the tail will dipolarize the near Earth magnetic field by transporting magnetic flux towards Earth and thus broaden the current sheet and prevent reconnection. There are no extended x-lines in the near Earth region for Run Mid, which is consistent with observations of most substorms.

A crucial caveat to this conclusion is that we expect smaller scale and shorter lived x-lines to appear in regions with a tailward flow. As the reconnection exhaust from the primary x-line in the midtail region reaches the stronger magnetic field near Earth and

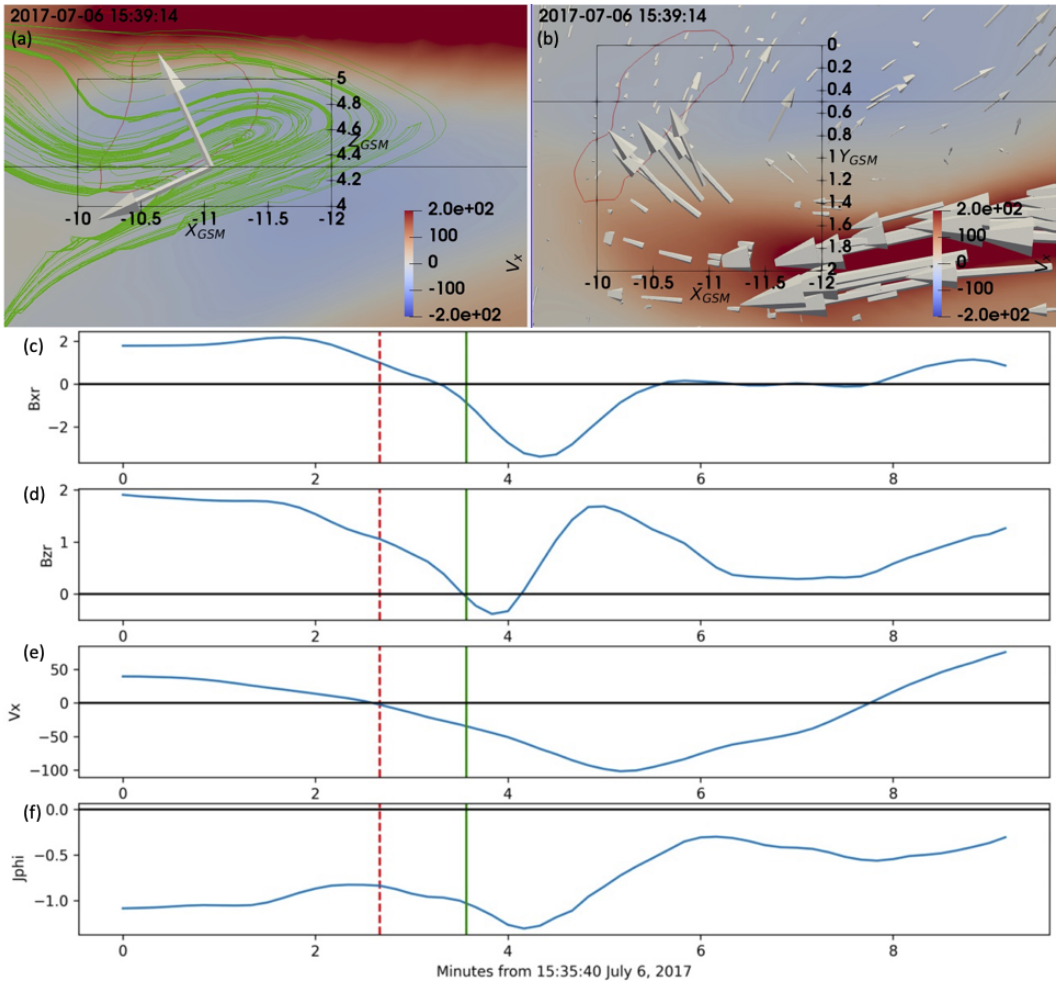

Figure 5. Panels (a) and (b) are similar to Fig. 3 (c) and (d) but zoomed in to show a near Earth x-line at an earlier time. The two tilted axes in panel (a) illustrate the "reconnection" axes for this x-line. Panels (c)-(f) show the reconnecting field ($B_{x,r}$), the reconnected field ($B_{z,r}$), $V_{X,GSM}$, and the azimuthal current in the GSM coordinate system respectively. These quantities are plotted vs time for the position of the x-line as indicated by the origin of the "reconnection" axes ($[x, y, z] = [-11.05, 0.5, 4.31]$). The horizontal black line shows 0 for each quantity, the vertical red dashed line marks the switch from Earthward to tailward flow, and the vertical green line marks when reconnection is observed.

rebounds tailward, the magnetic field is stretched due to the frozen in condition. This stretching of the magnetic field is highly localized in the dawn-dusk direction, limited to $\sim 5R_E$ at most, and it can create x-lines that last on the order of ~ 10 minutes. Thin current sheets have been observed as part of the rebounding process (Panov et al., 2010; ?, ?) and they could lead to reconnection in a similar manner. However, to the authors' knowledge, these x-lines have not been directly observed. Due to their small nature both in time and space it would be rare for a satellite to obtain in situ measurements showing these x-lines. If these x-lines do form near Earth, they could play an important role in the production of energetic particles. As argued by Angelopoulos et al. (2020), the average energy per particle is much higher closer to Earth than it is where typical x-lines form due to the X_{GSM} dependence of the magnetic field strength. Thus even small scale x-lines could potentially create very energetic particles. This topic will also need to be explored with test particles in a future paper

Note that both near-mid tail X-lines (Run DM) and midtail X-lines (Run Mid) are observed in the DM analysis of substorms (Stephens et al., 2022). In our future simulations we plan to use the DM output with 5-min cadence to incorporate the whole empirical story of X-lines into Gamera simulations. Further efforts will be necessary to also reproduce the multiscale non-MHD structure of the tail current sheet prior to reconnection onsets.

Appendix A Average flows in near Earth secondary x-lines

Fig. A1 shows the maximum (red), average (black), and minimum (blue) velocity in the X_{GSM} direction for each group of x-lines identified in Run Mid that is closer than $20R_E$ in the tail to Earth. Note, that the average velocity of all these x-lines is $\sim -17m/s$. It is important to keep in mind that if the x-lines form in rebounding flows they will be close to the Earthward flow as can be seen in Fig. 3 (d). Since the x-line identification method inherently overestimates the area the x-line occupies we can naturally expect some of the identified "x-lines" to be in the Earthward flow. This explains why the maximum velocity is often Earthward if the x-line forms in tailward flows. However, the average velocity is typically negative further confirming that the x-lines do form in tailward flows.

Appendix B Open Research

The data used in the study are archived on Zenodo (http://doi.org/10.5281/zenodo.7057795).

Acknowledgments

This work was funded by NASA grants 80NSSC20K1271 and 80NSSC20K1787, as well as the NSF grant AGS-1744269. We also acknowledge support from the NASA DRIVE Center, Center for Geospace Storms. Joachim Birn acknowledges support by NASA gran 80NSSC18K0834.

References

Angelopoulos, V., Artemyev, A., Phan, T. D., & Miyashita, Y. (2020). Near-earth magnetotail reconnection powers space storms. *Nature Physics*, *16*, 317-321.

Angelopoulos, V., McFadden, J., Larson, D., Carlson, C. W., Mende, S., Frey, H., ... Kepko, L. (2008). Tail reconnection triggering substorm onset. *Science*, *321*, 931-935.

Artemyev, A., Lu, S., El-Alaoui, M., Lin, Y., Angelopoulos, V., Zhang, X.-J., ... Russell, C. (2021). Configuration of the earth's magnetotail current sheet. *Geophysical Research Letters*, *48*.

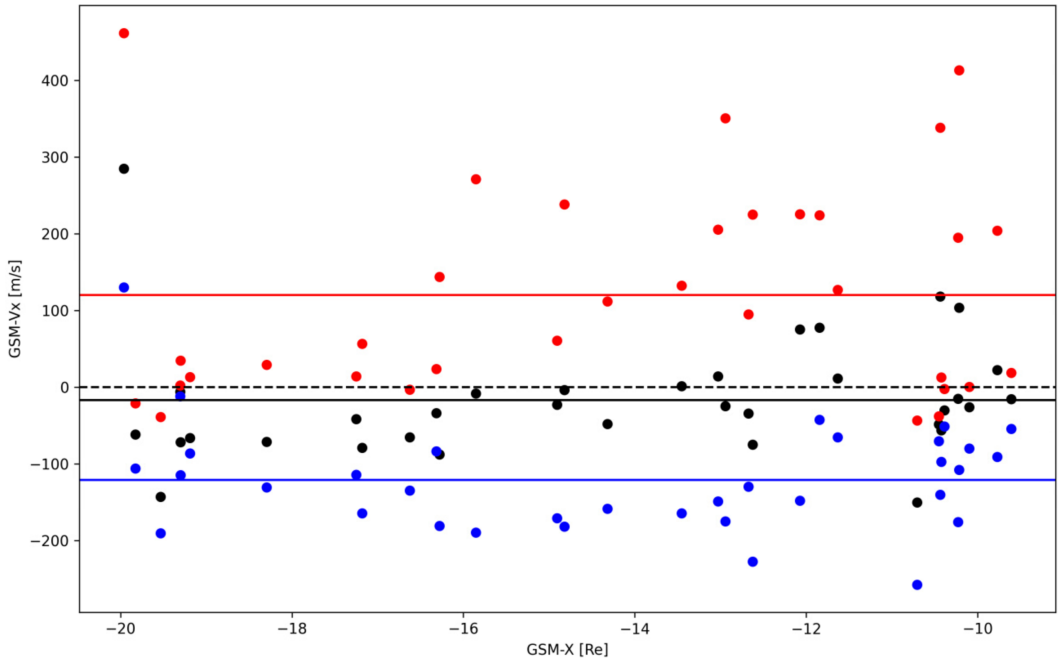

Figure A1. This shows the $V_{X,GSM}$ flow vs X_{GSM} position for all groups of x-lines identified within $20R_E$ of Earth in Run Mid. For each group we plot the maximum Earthward velocity (red), the mean velocity (black), and the minimum velocity (blue). The solid horizontal lines are the average of the maximum (red), mean (black), and minimum (blue) flows. The horizontal black and dashed line marks the difference between Earthward and tailward flows.

Baker, D., & P. (1996). Neutral line model of substorms: Past results and present view. *J. Geophys. Res.: Space Physics*, *101*, 12975-13010.

Bard, C., & Dorelli, J. (2021). Magnetotail reconnection asymmetries in an ion-scale, earth-like magnetosphere. *Annales Geophysicae*, *39*, 991-1003.

Bessho, N., & Bhattacharjee, A. (2014). Instability of the current sheet in the earth's magnetotail with normal magnetic field. *Physics of Plasmas*, *21*.

Birn, J., & Hesse, M. (2013). The substorm current wedge in mhd simulations. *Journal of Geophysical Research: Space Physics*, *118*, 3364-3376.

Birn, J., Hesse, M., & Schindler, K. (1996). Mhd simulations of magnetotail dynamics. *J. Geophys. Res.*, *101*, 12939-12954.

Birn, J., & Schindler, K. (2002). Thin current sheets in the magnetotail and the loss of equilibrium. *J. Geophys. Res.*, *107*.

Coppi, B., Laval, G., & Pellat, R. (1966). Dynamics of the geomagnetic tail. *Physical Review Letters*, *16*.

El-Alaoui, M., Ashour-Abdalla, M., Walker, R., Peroomian, V., Richard, R., Angelopoulos, V., & Runov, A. (2009). Substorm evolution as revealed by themis satellites and a globalmhd simulation. *Journal of Geophysical Research*, *114*.

Gong, F., Yu, Y., & Cao, J. (2021). Simulating the responses of the magnetosphere–ionosphere system to the imf by reversal. *Front. Phys.*, *10*.

Hesse, M., & Birn, J. (1994). Mhd modeling of magnetotail instability for localized resistivity. *Journal of Geophysical Research*, *99*(A5), 8565-8576.

Hesse, M., & Schindler, K. (2001). The onset of magnetic reconnection in the magnetotail. *Earth, Planets and Space*, *53*, 645-653.

Imber, S. M., Slavin, J. A., Auster, H. U., & Angelopoulos, V. (2022). A themis survey of flux ropes and traveling compression regions: Location of the near-earth

reconnection site during solar minimum. *Journal Of Geophysical Research: Space Physics*, *116*.

Liu, Y.-H., Birn, J., Daughton, W., Hesse, M., & Schindler, K. (2014). Onset of reconnection in the near magnetotail: Pic simulations. *Journal of Geophysical Research: Spacec Physics*, *119*, 9773-9789.

Merkin, V. G., & Lyon, J. G. (2010). Effects of the low-latitude ionospheric boundary condition on the global magnetosphere. *Journal of Geophysical Research: Space Physics*, *115*.

Merkin, V. G., Panov, E. V., Sorathia, K. A., & Ukhorskiy, A. Y. (2019). Contribution of bursty bulk flows to the global dipolarization of the magnetotail during an isolated substorm. *Journal of Geophsyical Research: Space Physics*, *124*.

Min, K., Okuda, H., & Sato, T. (1985). Numerical studies on magnetotail formation and driven reconnection. *Journal of Geophysical Research: Space Physics*, *90*, 4035-4045.

Nagai, T., Fujimoto, M., Saito, Y., Machida, S., Terasawa, T., Nakamura, R., ... Kokubun, S. (1998). Structure and dynamics of magnetic reconnection for substorm onsets with geotail observations. *Journal of Geophysical Research: Space Physics*, *103*, 4419-4440.

Nakamura, R., Baumjohann, W., Runov, A., Volwerk, M., Zhang, T. L., Klecker, B., ... Frey, H. U. (2002). Fast flow during current sheet thinning. *Geophysical Research Letters*, *29*.

Ohtani, S., Miyashita, Y., Singer, H., & Mukai, T. (2009). Tailward flows with positive bz in the near-earth plasma sheet. *Journal of Geophysical Research*, *114*.

Panov, E. V., Nakamura, R., Baumjohann, W., Sergeev, V. A., Petrukovich, A. A., Angelopoulos, V., ... Larson, D. (2010). Plasma sheet thickness during a bursty bulk flow reversal. *J. Geophys. Res.*, *115*.

Park, K. (2021). Global mhd simulation of the weak southward imf condition for different time resolutions. *Front. Astron. Space Sci.*, *8*.

Pritchett, P. L. (2015). Structure of exhaust jets produced by magnetic reconnection localized in the out-of-plane direction. *Journal of Geophysical Research*, *120*, 592-608.

Raeder, J. (1999). Modeling the magnetosphere for northward interplanetary magnetic field: Effects of electrical resistivity. *Journal of Geophsyical Research: Space Physics*, *104*.

Raeder, J. (2003). Global geospace modeling: Tutorial and review. space plasma simulation. *Lect. Notes Phys.*, *615*, 212-246. (Edited by J. Büchner, C. Dum, and M. Scholer)

Raeder, J., Berchem, J., & Ashour-Abdalla, M. (1996). The importance of small scale processes in global mhd simulations: Some numerical experiments. *The Physics of Space Plasmas*, *14*, 403. (Edited by T. Chang and j. R. Jasperse)

Raeder, J., McPherron, R. L., Frank, L. A., Paterson, W. R., Sigwarth, J. B., Lu, G., ... Slavin, J. A. (2001). Global simulation of the geospace environment modeling substorm challenge event. *J. Geophys. Res.*, *106*.

Rogers, A. J., Farrugia, C. J., & Torbert, R. B. (2019). Numerical algorithm for detecting ion diffusion regions in the geomagnetic tail with applications to mms tail season 1 may to 30 september 2017. *Journal of Geophysical Research: Space Physics*, *124*, 6487-6503.

Runov, A., Grandin, M., Palmroth, M., Battarbee, M., Ganse, U., Hietala, H., ... Turner, D. (2021). Ion distribution functions in magnetotail reconnection: global hybrid-vlasov simulation results. *Ann. Geophys.*, *39*, 599-612.

Runov, A., Nakamura, R., Baumjohann, W., Zhang, T. L., Volwerk, M., Eichelberger, H.-U., & Balogh, A. (2003). Cluster observation of a bifurcated current sheet. *Geophysical Research Letters*, *30*.

Runov, A., Sergeev, V. A., Baumjohann, W., Nakamura, R., Apatenkov, S., Asano, Y., ... Rème, H. (2005). Electric current and magnetic field geometry in

flapping magnetotail current sheets. *Annales Geophysicae*, *23*, 1391-1403.
Runov, A., Sergeev, V. A., Nakamura, R., Baumjohann, W., Apatenkov, S., Asano, Y., ... Balogh, A. (2006). Local structure of the magnetotail current sheet: 2001 cluster observations. *Annales Geophysicae*, *24*, 247-262.
Russell, C. T., & McPherron, R. L. (1973). The magnetotail and substorms. *Space Sciences Reviews*, *15*, 205-266.
Schindler, K. (1974). A theory of the substorm mechanism. *Journal of Geophsyical Research: Space Physics*, *79*.
Scholer, M., & Otto, A. (1991). Magnetotail reconnection: Current diversion and field-aligned currents. *Geophysical Research Letters*, *18*, 733-736.
Sergeev, V., Angelopoulos, V., Kubyshkina, M., Donovan, E., Zhou, X.-Z., Runov, A., ... Nakamura, R. (2011). Substorm growth and expansion onset as observed with ideal ground-spacecraft themis coverage. *Journal of Geophysical Research: Space Physics*, *116*.
Sergeev, V., Runov, A., Baumjohann, W., Nakamura, R., Zhang, T. L., Volwerk, M., ... Klecker, B. (2003). Current sheet flapping motion and structure observed by cluster. *Geophysical Research Letters*, *30*.
Sitnov, M. I., Buzulukova, N., Swisdak, M., Merkin, V. G., & Moore, T. E. (2013). Spontaneous formation of dipolarization fronts and reconnection onset in the magnetotail. *Geophsyical Research Letters*, *40*.
Sitnov, M. I., & Schindler, K. (2010). Tearing stability of a multiscale magnetotail current sheet. *Geophsyical Research Letters*, *37*.
Sorathia, K. A., Merkin, V. G., Panov, E. V., Zhang, B., Lyon, J. G., & Garretson, e. a., J. (2020). Ballooning-interchange instability in the near-earth plasma sheet and auroral beads: Global magnetospheric modeling at the limit of the mhd approximation. *Geophys. Res. Lett.*, *47*.
Stephens, G., Sitnov, M., Korth, H., Tsyganenko, N. A., Ohtani, S., Gkioulidou, M., & Ukhorskiy, A. Y. (2019). Global empirical picture of magnetospheric substorms inferred from multimission magnetometer data. *Journal of Geophysical Research: Space Physics*, *124*, 1085-1110.
Stephens, G. K., Sitnov, M. I., Weigel, R. S., Turner, D. I., Tsyganenko, N. A., Rogers, A. J., ... Slavin, J. A. (2022). Global structure of magnetotail reconnection revealed by mining space magnetometer data. *Earth and Space Science Open Archive*. doi: 10.1002/essoar.10511996.1
Torbert, R. B., Burch, J. L., Phan, T. D., Hesse, M., Argall, M. R., Shuster, J., & Ergun, R. E. e. a. (2018). Electron-scale dynamics of the diffusion region during symmetric magnetic reconnection in space. *Science*, *362*, 1391-1395.
Ugai, M., & Tsuda, T. (1979). Magnetic field-line reconnexion by localized enhancement of resistivity. part 4. dependence on the magnitude of resistivity. *Journal of Plasma Physics*, *22*, 1-14.
Zhang, B., Sorathia, K., Lyon, J., Merkin, V., Garretson, J., & Wiltberger, M. (2019). Gamera: A three-dimensional finite-volume mhd solver for non-orthogonal curvilinear geometries. *The Astrophysical Journal*, *244*.
Zhang, L. Q., Liu, Z. X., Ma, Z. W., Baumjohann, W., Pu, Z. Y., Dunlop, M. W., ... Wang, J. Y. (2010). X line distribution determined from earthward and tailward convective bursty flows in the central plasma sheet. *Journal of Geophysical Research*, *115*.
Zhao, S., Tian, A., Shi, Q., Xizo, C., Fu, S., Zong, Q., ... Tan, K. (2016). Statistical study of magnetotail flux ropes near the lunar orbit. *Science China Technological Sciences*, *59*, 1591-1596.